Structure
Article

Electron Cryomicroscopy Comparison of the Architectures of the Enveloped Bacteriophages ϕ6 and ϕ8

Harri T. Jäälinoja,[1,2] Juha T. Huiskonen,[1,2] and Sarah J. Butcher[1,2,3,*]
[1] Centre of Excellence in Virus Research and Institute of Biotechnology
[2] Department of Biological and Environmental Sciences, P.O. Box 65 (Viikinkaari 1), University of Helsinki, FI-00014 Helsinki, Finland
[3] Lab address: http://www.biocenter.helsinki.fi/bi/butcher/
*Correspondence: sarah.butcher@helsinki.fi
DOI 10.1016/j.str.2006.12.004

SUMMARY

The enveloped dsRNA bacteriophages ϕ6 and ϕ8 are the two most distantly related members of the *Cystoviridae* family. Their structure and function are similar to that of the *Reoviridae* but their assembly can be conveniently studied in vitro. Electron cryomicroscopy and three-dimensional icosahedral reconstruction were used to determine the structures of the ϕ6 virion (14 Å resolution), ϕ8 virion (18 Å resolution), and ϕ8 core (8.5 Å resolution). Spikes protrude 2 nm from the membrane bilayer in ϕ6 and 7 nm in ϕ8. In the ϕ6 nucleocapsid, 600 copies of P8 and 72 copies of P4 interact with the membrane, whereas in ϕ8 it is only P4 and 60 copies of a minor protein. The major polymerase complex protein P1 forms a dodecahedral shell from 60 asymmetric dimers in both viruses, but the α-helical fold has apparently diverged. These structural differences reflect the different host ranges and entry and assembly mechanisms of the two viruses.

INTRODUCTION

Viral capsid structures, protecting the viral nucleic acid, have been frequently studied as paradigms for protein-protein interactions. Icosahedral virus capsids represent some of the largest yet simplest macromolecular complexes that have been studied to date. Often the main function of the capsid is to act as a container delivering the viral genome into the cell. Thus, the capsid components mainly have a structural role. However, the double-stranded RNA (dsRNA) viruses always keep their genome within the capsid. Hence the capsid not only serves to protect the RNA but is also a molecular machine, carrying the viral enzymes required for packaging, replicating, and transcribing RNA. We are interested in the structure, assembly, and regulation of these machines.

Members of the *Cystoviridae* family (ϕ6–ϕ14) are enveloped bacteriophages with segmented dsRNA genomes (Mindich et al., 1999; Vidaver et al., 1973). The dsRNA genomes are divided into three segments: the small (S), medium (M), and large (L) segment. The L segment encodes four proteins (P1, P2, P4, and P7) that assemble into an icosahedrally symmetric polymerase complex (PC; Figure 1). The PC can package positive, single-stranded RNA, replicate it to dsRNA, and transcribe new positive-sense RNA. Thus, this family of viruses has proven to be a valuable model system to study dsRNA viral assembly (Gottlieb et al., 1990), packaging of a segmented RNA genome (Mindich, 2004), the RNA translocation process (Lisal et al., 2004; Lisal and Tuma, 2005; Mancini et al., 2004), and RNA replication (Butcher et al., 2001; Makeyev and Bamford, 2000a, 2000b; Yang et al., 2001, 2003). ϕ6 and ϕ8 are the only two *Cystoviridae* where in vitro assembly has been studied (Kainov et al., 2003a; Poranen et al., 2001; Poranen and Tuma, 2004).

ϕ6 was the first cystovirus to be isolated (Vidaver et al., 1973), and it is the best-characterized member of the *Cystoviridae* family. The organization of ϕ6 is shown schematically in Figure 1. The ϕ6 PC is mainly formed of 120 copies of P1 (Huiskonen et al., 2006a). Twelve P4 hexamers protrude from the PC vertices (Huiskonen et al., 2006b). A nucleocapsid (NC) shell, formed of 200 P8 trimers (T = 13*l* organization), partially covers the PC (Butcher et al., 1997; de Haas et al., 1999; Huiskonen et al., 2006a). The NC is enveloped by a lipid membrane where the lipids are derived from the host cytoplasmic membrane (Laurinavicius et al., 2004; van Etten et al., 1976). The spike protein P3 protrudes from the membrane, where it is anchored by the integral membrane protein P6 (Stitt and Mindich, 1983; van Etten et al., 1976).

The ϕ6 replication cycle has been recently reviewed (Poranen et al., 2005). ϕ6 infection starts when P3 attaches to a type IV pilus of the host (Bamford et al., 1976; Romantschuk and Bamford, 1985). P6 causes the ϕ6 membrane to fuse with the host outer membrane, and the NC is released into the periplasm (Bamford et al., 1987). A viral endopeptidase (P5) digests the cell wall (Caldentey and Bamford, 1992; Hantula and Bamford, 1988). The P8 shell is necessary for penetration of the NC through the cytoplasmic membrane, and disassembles on entry (Romantschuk et al., 1988). In the cytoplasm, the released PCs start transcribing, eventually leading to the

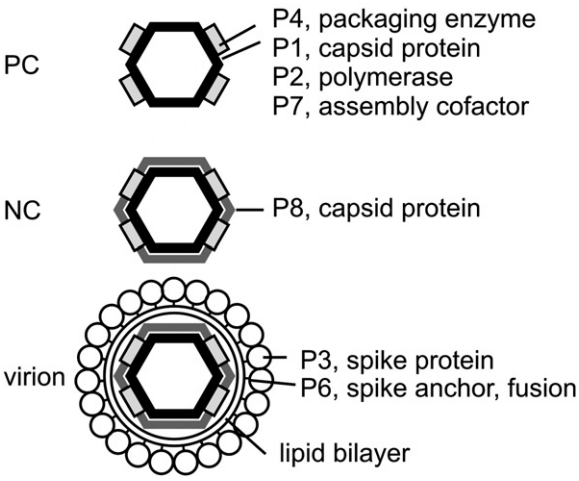

Figure 1. Schematic Representation of the ϕ6 Polymerase Complex, Nucleocapsid, and Virion
The major components discussed in the paper are labeled.

assembly of new viruses (Bamford and Mindich, 1980; Kakitani et al., 1980).

Recently, additional cystoviruses have been isolated (ϕ7–ϕ14; Mindich et al., 1999). Based on sequence comparison among the members of the *Cystoviridae*, ϕ8, ϕ12, and ϕ13 are distant relatives of ϕ6, with ϕ8 being the most remote (Gottlieb et al., 2002a, 2002b; Hoogstraten et al., 2000; Qiao et al., 2000). This reflects differences in the host specificity of ϕ6 and its distant relatives. Whereas ϕ6 infects *Pseudomonas syringae* pv. *phaseolicola*, ϕ8, ϕ12, and ϕ13 also infect other Gram-negative hosts such as *Escherichia coli* and *Salmonella typhimurium* (Mindich et al., 1999). Several differences in the infection mechanism explain the different host ranges. First, ϕ6 binds to type IV pili, but ϕ8, ϕ12, and ϕ13 bind directly to a truncated lipopolysaccharide O chain in the host outer membrane. Second, the attachment specificity proteins also differ: in ϕ8, the spike protein consists of two peptides, P3a (59 kDa) and P3b (41 kDa), whereas in ϕ6, P3 is a single polypeptide chain (69 kDa; Gottlieb et al., 2002b; Hoogstraten et al., 2000; Qiao et al., 2000; Stitt and Mindich, 1983). Third, the penetration of the plasma membrane is mediated by P8 in ϕ6 (Daugelavicius et al., 2005; Olkkonen et al., 1990) but by the PC proteins in ϕ8 (Sun et al., 2003). Initial studies have indicated that in ϕ8, P8 is a membrane-associated protein (Hoogstraten et al., 2000; Sun et al., 2003).

Structural information from different cystoviruses would help the integration of experimental biochemical and genetic data obtained from different members of the family and thus promote understanding of the viral life cycles. Although the architecture of the ϕ6 nucleocapsid has been resolved to 7.5 Å resolution (Huiskonen et al., 2006a), the membrane organization of this major group of viruses has not been addressed. In addition, it is still not clear what the level of structural conservation is within the *Cystoviridae* and among them and other dsRNA virus families such as the *Reoviridae* and *Birnaviridae*.

To shed light on the structures which may be responsible for the differences in host cell entry in the cystoviruses, we chose to study the two most distantly related members of the family, ϕ6 and ϕ8, as these two were expected to provide the most valuable comparison. We have determined the structure of the ϕ6 and ϕ8 virions and the ϕ8 core (PC containing dsRNA) using electron cryomicroscopy (cryo-EM) and three-dimensional (3D) image reconstruction (Adrian et al., 1984; Baker et al., 1999; Crowther, 1971). Comparison of the ϕ6 and ϕ8 virion reconstructions allows us to address the role and organization of the membrane proteins and P8 from a structural point of view. Also, our 8.5 Å resolution reconstruction of the ϕ8 PC clearly reveals the organization of the major capsid protein P1, allowing a detailed comparison with other dsRNA viruses (Grimes et al., 1998; Huiskonen et al., 2006a; Naitow et al., 2002; Nakagawa et al., 2003; Prasad et al., 1996; Reinisch et al., 2000).

RESULTS

Choice of Strategy for Complex Particle Reconstruction

There are many examples in the literature where dissociated particles or recombinant subviral particles have been used to define different steps in virus assembly, or to delineate different components within a complex viral particle. This is especially the case in image processing of membrane-containing viruses—we like to avoid the membrane as it is often not so well defined, thus adding noise and lowering the resolution of the reconstruction (Bottcher et al., 1997; Butcher et al., 1995, 1997; Conway et al., 1997; Dryden et al., 2006; Zhou et al., 1995). However, the dissociation potentially removes loosely associated proteins or causes conformational changes that affect our interpretation (Grünewald et al., 2003; Trus et al., 1999; Zhou et al., 1999). Here we exploited detergent extraction of the ϕ8 virion to delineate the proteins of the dsRNA-containing PC (core), but we also used a holistic approach, studying the purified ϕ6 and ϕ8 virions to extract additional information for their structural comparison.

Electron Cryomicroscopy and Image Reconstruction

Purified ϕ6 virions and ϕ8 virions and cores were subjected to cryo-EM and 3D image reconstruction. In the electron micrographs, all of the particles were similar to those described previously (Kenney et al., 1992; Yang et al., 2003). A temperature-dependent phenomenon has been noticed with ϕ6, where optimal incorporation of P3 and P6 occurs in a range between 18°C and 24°C, with a 75% reduction at 28°C (Mindich et al., 1979). The ϕ6 for this study was thus grown at 23°C to maximize the spike protein content. In ϕ8, we found that at 15°C we had good incorporation of the spikes, and that this also correlated with virions where the membranes closely followed the outline of the nucleocapsid as judged by electron microscopy.

Table 1. Reconstruction Statistics

	ϕ6 Virion	ϕ8 Virion	ϕ8 Core
Number of particles	517	992	12,867
Number of micrographs	23	60	66
Nominal sampling (Å/pixel)	2.8	2.8	1.4
Micrograph underfocus (μm)	1.3–2.9	0.8–3.3	0.7–3.3
Resolution of P1 shell[a] (Å)	14	18	8.5
Resolution of P8 shell[a] (Å)	14	–	–
Resolution of membrane[a] (Å)	24	21	–
Overall resolution of particle[a] (Å)	18	21	8.7

[a] An estimate for the resolution based on the Fourier shell correlation 0.5 criterion.

Reconstruction statistics and resolution estimates for different radial regions of the reconstructions are shown in Table 1. The resolution varies depending on the icosahedral order in the structure (Huiskonen et al., 2004). Figure S1 (see the Supplemental Data available with this article online) shows in detail the resolution estimates for the best defined region, the PC shell. The maximum resolution was 14 Å for the ϕ6 virion, 18 Å for the ϕ8 virion, and 8.5 Å for the ϕ8 core. Central sections of the reconstructions are shown for comparison of the ϕ6 virion (Figure 2A, ϕ6v), ϕ8 virion (Figure 2A, ϕ8v), and ϕ8 core (Figure 2B).

Comparison between ϕ6 and ϕ8 Revealed Differences in Their Overall Organization

Reconstructions of ϕ6 and ϕ8 virions revealed multilayered structures consisting of spike proteins, membrane, one or two protein shells, and several layers of RNA (Figure 2). The layers were assigned based on previously published structures of ϕ6 and the ϕ8 core reconstruction presented here (Butcher et al., 1997; de Haas et al., 1999; Huiskonen et al., 2006a). The number and position of the outer layers vary between the two virions. First, the spike layer extends further out in ϕ8 than in ϕ6 (Figure 2A, pink lines). Measured from the outer membrane bilayer, the ϕ6 spike is 2 nm tall and the ϕ8 spike is 7 nm tall. In addition, the membrane bilayer is much better defined in the ϕ8 reconstruction than in that of ϕ6. In ϕ8, both the inner (Figure 2A, magenta line) and outer (Figure 2A, orange line) leaflets are clearly visible. Measurement of the average membrane thickness (Laurinmäki et al., 2005) indicated a 2.8 nm separation between the leaflets. However, individual spikes and any transmembrane structures were unresolved in the icosahedrally averaged reconstructions.

The nucleocapsid interactions with the membrane in ϕ6 differ from those in ϕ8 (Figures 2C and 3). In ϕ6, they are mediated mainly by a layer of P8 trimers organized on a T = 13/ icosahedral lattice interrupted at the 5-fold vertices by rings of protein P4 (Figure 2A, yellow and green radii; Figures 2C, 3A, and 3B; Butcher et al., 1997; Huiskonen et al., 2006a). An equivalent T = 13/ layer was clearly missing in ϕ8 (Figures 2C, 3A, and 3B). Instead, P4 hexamers (Kainov et al., 2003b) contact the membrane at the vertices along with 60 copies of a minor, ~11 kDa protein on the facet (Figures 2C and 3B, ϕ8v, red circle). This minor protein was not present in the ϕ8 core reconstruction (Figure 3B, ϕ8c; Figure 4A), suggesting that it is loosely bound to the PC shell and removed with the membrane when the cores are prepared from the virions by detergent extraction. Hence it is a putative membrane-associated protein. The presence of this minor protein in ϕ8 prompted us to look for additional density in the ϕ6 virion at the radii of the nucleocapsid that might have been lost from the isolated ϕ6 nucleocapsids due to detergent treatment. We noticed that the P8 peripheral domain is better ordered in the ϕ6 virion reconstruction than in the ϕ6 nucleocapsid reconstruction (Figure 3A, ϕ6v and ϕ6nc). This is especially evident for the P8 trimers that interact with the P4 hexamer (Figure 3A, ϕ6v, red circle; Huiskonen et al., 2006a).

The Overall Polymerase Complex Architecture Is Conserved between ϕ6 and ϕ8

Despite the differences in the outer layers, the PCs of ϕ6 and ϕ8 were similar in their overall size, shape, and quaternary organization (Figure 2A, red and blue lines; Figures 3C and 3D). The average spacing of the RNA shells from ϕ8 is 2.9 nm, compared to 3.1 nm in ϕ6 (Huiskonen et al., 2006a). No obvious density for the polymerase or P7 was seen in either virus. The P4s are hexameric (de Haas et al., 1999; Kainov et al., 2003b), sitting on the icosahedral 5-fold axis of symmetry, so they are incorrectly averaged in the reconstruction. Hence they appear as blurred densities containing no distinguishing features compared to the well-defined PC shell (Figures 2–4). In the ϕ8 core reconstruction, the P4 appears to have C5, not C30, symmetry, which would be expected for a C6 object after applying C5 symmetry. This suggests that the P4 is actually asymmetric and the C5 symmetry arises from the reconstruction process. Alternative methods to icosahedral reconstruction are thus needed to describe its shape and interaction with P1. We have recently addressed the interaction between ϕ8 P4 and the P1 shell using a vertex reconstruction method (Huiskonen et al., 2006b).

The high-resolution reconstruction of the ϕ8 core (Figure 2B; Figure 3, ϕ8c; Figure 4A) revealed individual P1 monomers organized on a dodecahedral framework similar to that in the ϕ6 PC shell (Figures 3C and 3D). At 8.5 Å resolution, it was possible to manually demarcate the subunit boundaries and segment the PC shell density. We identified two monomers in the icosahedral asymmetric unit, P1A (Figure 4, blue density) and P1B (Figure 4, red density). The ϕ8 PC shell is thus composed of 120 copies of P1, with two copies in each asymmetric unit (Figure 3D; see below), similar to ϕ6 (Huiskonen et al., 2006a). P1A monomers are located around the 5-fold axis of

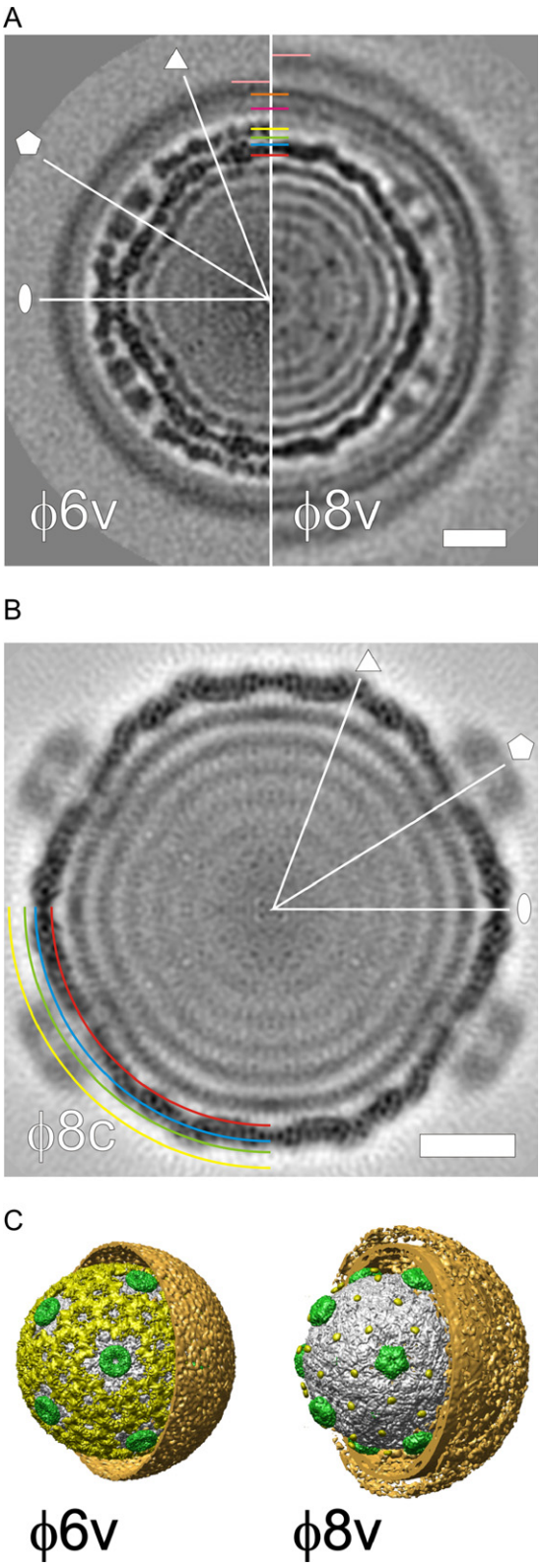

Figure 2. Central Sections and Isosurface Representations of ϕ6 and ϕ8 Reconstructions

(A) Central cross-sections of ϕ6 (left) and ϕ8 (right) virion reconstructions. One of the icosahedral 2-fold (ellipse), 3-fold (triangle), and 5-fold (pentagon) axes of symmetry is indicated. Some radii are indicated with circle segments colored in red (PC, 23 nm), blue (PC, 25 nm), green (NC, 26 nm), yellow (NC, 27 nm), magenta (inner leaflet, 30 nm), orange (outer leaflet, 33 nm), and pink (ϕ6 spikes, 35 nm; ϕ8 spikes, 37 nm). The scale bar represents 10 nm.

(B) Central cross-section of the ϕ8 core reconstruction. The icosahedral axes of symmetry and some radii are indicated as in (A). The scale bar represents 10 nm. Positive density is black in (A) and (B).

(C) Isosurface representations of the ϕ6 and ϕ8 virion structures each viewed down a 5-fold axis of symmetry. The high-resolution reconstructions were used for the ϕ6 NC and the ϕ8 core; the membranes came from the virion reconstructions. P1 is colored gray and P4 is green. ϕ6 P8 and the putative membrane-associated protein of ϕ8 are colored yellow. The protein layers are thresholded at 2σ above the mean. The membrane and spike layers (brown) are thresholded at 1σ above the mean.

symmetry, and P1B monomers around the 3-fold axis of symmetry (Figure 4A).

The individual ϕ8 P1 monomers are similar in their overall shape, and revealed tubular structures that we interpret as α helices (Figure 4B, yellow barrels). We assigned 14 putative helices computationally using helixhunter (Jiang et al., 2001). The overall helix length distribution had a minimum of 5, a maximum of 26, and a median of 8 residues. The helices are clustered in three domains. A secondary-structure prediction indicated a primarily α-helical content with 24 helices and some β sheet (Figure S2) (Cuff and Barton, 2000). The discrepancy could be due to both the limited resolution of the reconstruction and the reliability of the secondary-structure prediction.

The demarcation of molecular boundaries in the core reconstruction also revealed the positions of other proteins in relation to the P1 monomers. First, 12 rings of P4 protein interact with P1A monomers, but not with P1B monomers (Figure 4A, green densities). Second, the putative membrane-associated protein between the core and the membrane layer is located on the boundary between P1A and P1B (Figure 4B).

The Tertiary-Structure Comparison of ϕ6 and ϕ8 P1s Reveals Significant Differences

Determination of the helix positions enabled detailed comparison of the P1 tertiary structures—on the one hand between the two monomers within the same virus, and on the other hand between ϕ6 and ϕ8 (Figure 5A). We have quantified the similarity of the P1 helices within both viruses. We calculated the rmsd value between the endpoints of the helices: the value is 4.4 Å for ϕ6 helices and 4.7 Å for ϕ8 helices. This shows that the conformational differences are about the same within both viruses. Because the P1s from the two viruses are quite different at the tertiary structure level, we cannot quantify the similarity between the two viruses. For this we would need to be able to say which helices correspond to each other, but this was not possible.

Although the identified helices within a dimer can thus be readily superimposed, the ϕ6 monomer density or the modeled helices cannot be superimposed on those of ϕ8. This suggests that the tertiary structures of ϕ6 P1 and ϕ8 P1 are markedly different even though the

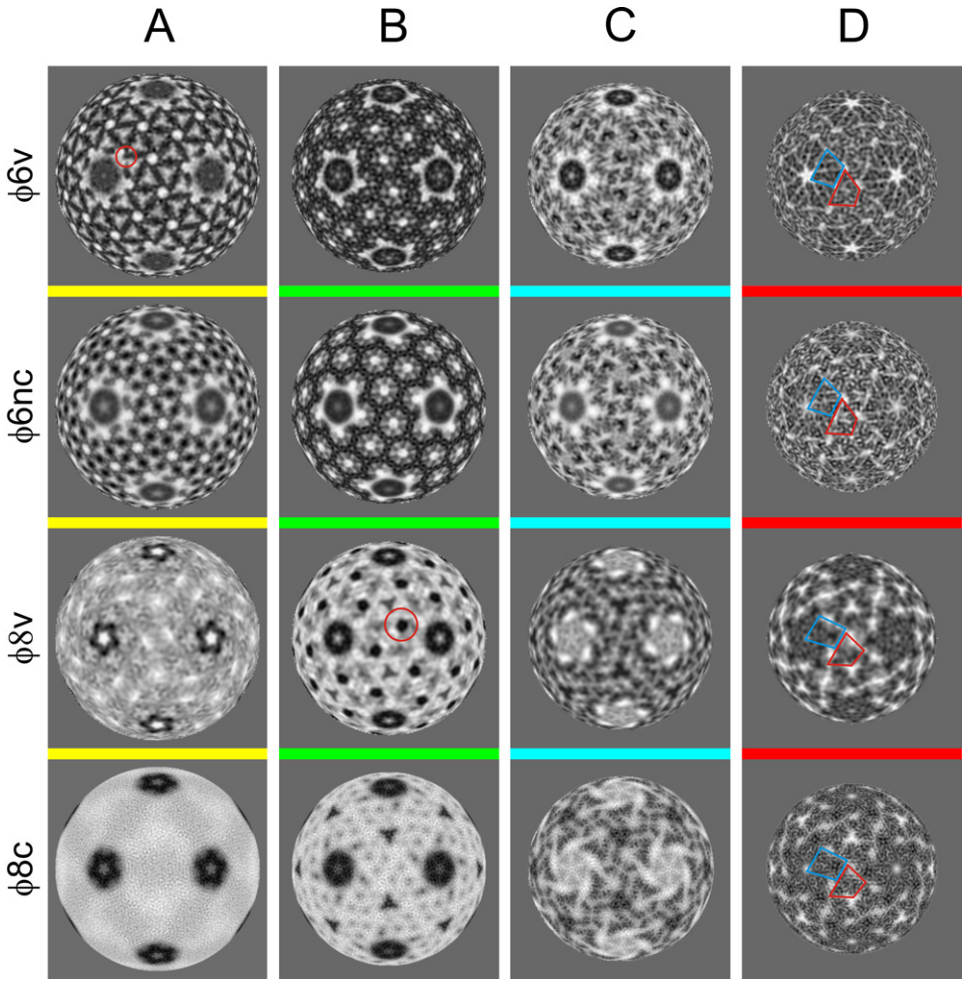

Figure 3. Radial Shells of the Reconstructions

Selected spherical cross-sections are shown for the ϕ6 virion (ϕ6v), ϕ6 nucleocapsid (ϕ6nc; EMD, EBI accession number EMD-1206), ϕ8 virion (ϕ8v), and ϕ8 core (ϕ8c). The sections were taken at the following radii: (A) 27 nm, (B) 26 nm, (C) 25 nm, and (D) 23 nm. Additional densities seen in the ϕ6v compared to the ϕ6nc and in the ϕ8v compared to the ϕ8c are indicated for one asymmetric unit with red circles on ϕ6v and ϕ8v. P1A subunits are outlined in blue and P1B subunits in red. Sections are 2.8 Å thick. Positive density is black.

assembled shells have a similar appearance (Figure 5B). We also compared the unassigned densities in the maps (Figures 5C and 5D) to ensure that these were not responsible for the differences observed.

DISCUSSION

We have studied here the structure of the icosahedral membrane-containing viruses ϕ6 and ϕ8, the two most distantly related members of the *Cystoviridae* family known to date. These cystovirus virion structures represent the first examples, to our knowledge, of membrane-containing bacteriophages where an icosahedrally organized nucleocapsid is enveloped by a membrane within which there are proteins that do not follow icosahedral symmetry. Such an organization has been described previously in the members of the *Herpesviridae* family, which are enveloped viruses infecting vertebrates (Grünewald et al., 2003; Trus et al., 1999; Zhou et al., 1999). In contrast, in the lipid-containing bacteriophages studied so far (PM2, PRD1, and Bam35), the membrane has been observed to reside under an icosahedrally ordered capsid (Abrescia et al., 2004; Huiskonen et al., 2004; Laurinmäki et al., 2005). These differences in membrane position reflect the different entry and assembly mechanisms of the viruses. In the members of the *Cystoviridae* family, the viral membrane is required to fuse with the host cell outer membrane in order to deliver the nucleocapsid into the periplasm, eventually leading to release of the PC into the cytoplasm. Similarly, in the *Herpesviridae* family, membrane fusion allows the release of the nucleocapsid and tegument into the cytoplasm for microtubule-directed transport to the nucleus, where DNA release occurs (Spear and Longnecker, 2003; Whittaker et al., 2000). In contrast, in PRD1 and Bam35, only the genome enters the cytoplasm (Grahn et al., 2006).

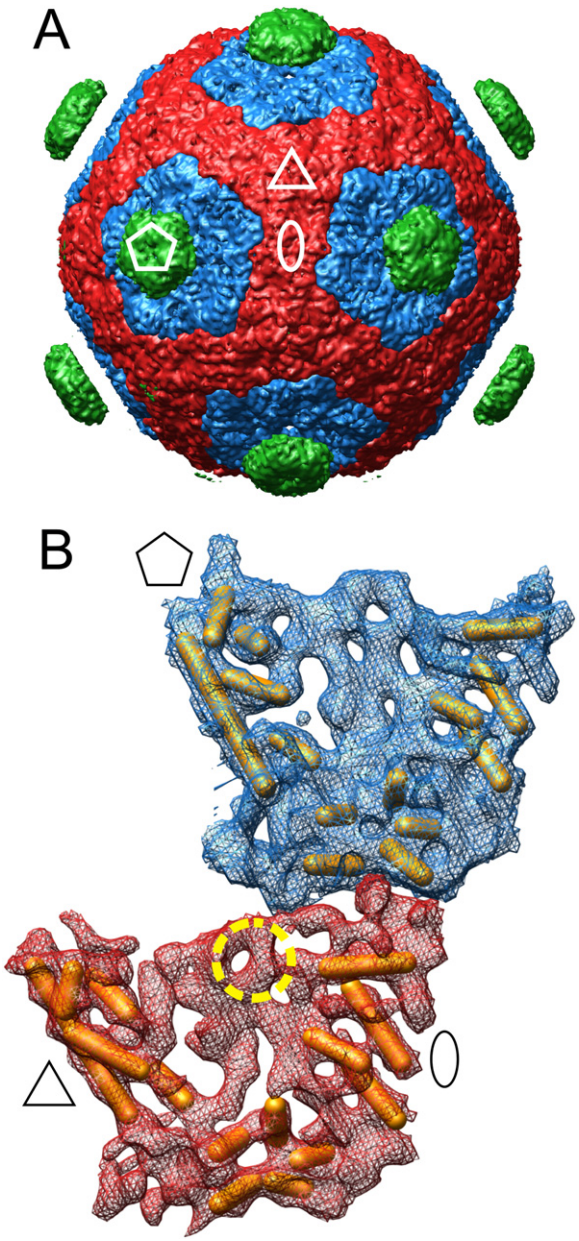

Figure 4. ϕ8 Polymerase Complex Architecture
(A) Isosurface rendering of the ϕ8 core. P1 subunits A are colored in blue and subunits B are in red. The packaging enzyme, P4, is colored in green. The isosurfaces were drawn at 2σ above the mean density level. (B) Assignment of putative α helices in P1. A mesh surface representation of subunit A is colored in blue and subunit B is in red. α helices are modeled as 0.5 nm thick rods (yellow). The approximate location of the putative membrane-associated protein is marked with a dashed yellow line. The isosurfaces were drawn at a high threshold (~3σ above the mean density) to reveal the structure in detail.

In the ϕ6 virion, we saw no stoichiometric relationship between the membrane proteins and the nucleocapsid. This reflects the fact that only one of the membrane proteins (P9) is essential for envelopment (Johnson and Mindich, 1994; Mindich et al., 1976) and the fact that the number of spikes (P3) attached to the fusion protein (P6) varies depending on the growth temperature (Mindich et al., 1979). In comparison, herpesvirus assembly is extremely complex, but there are some interesting analogies. In herpesvirus, nucleocapsids formed and packaged in the nucleus are released into the cytoplasm, where the majority of the tegument proteins are added. The tegument links the capsid and the envelope. Tegumentation initiates at two different sites, the capsid and the future site of envelopment. The capsid-proximal tegument proteins retain icosahedral order and stoichiometry but the outer tegument proteins do not. Assembly thus requires a complex network of interactions between nucleocapsid, tegument, and glycoproteins, in which some components are essential (Mettenleiter et al., 2006).

Comparison of the ϕ6 and ϕ8 Infection Pathways

The general organization of the outer layers in the ϕ6 and ϕ8 virions was found to differ in several aspects, reflecting not only very limited sequence identity but also functional differences in virus infection such as attachment to the host cell and penetration of the host cytoplasmic membrane. First, the length of the spikes differs. This is probably due to the fact that the receptor binding spike proteins are different (Bamford et al., 1976; Mindich et al., 1999). Second, interactions from the nucleocapsid to the membrane are coordinated through 200 trimers of P8 (16 kDa) in ϕ6, but through only 60 occurrences of a membrane-associated protein in ϕ8. Third, differences were observed in the ϕ6 and ϕ8 subviral particles that penetrate the host cytoplasmic membrane (ϕ6nc versus ϕ8c), emphasizing that the penetration step is radically different between the two viruses (Sun et al., 2003).

The membrane was more ordered in the ϕ8 virion than in ϕ6. More membrane protein species are important for the assembly of the membrane in ϕ8 than in ϕ6. Of the ϕ6 membrane proteins P3, P6, P9, P10, and P13, only P9 is needed for the membrane to assemble properly (Johnson and Mindich, 1994). In contrast, in ϕ8, at least P10, P3a, P3b, and PF are required (Hoogstraten et al., 2000). This indicates a greater degree of interaction between the membrane glycoproteins in ϕ8, which could explain the observed difference in membrane order.

In the ϕ8 virion reconstruction, additional density, designated as a putative membrane-associated protein, was attached to the PC at a unique site created by two P1 monomers. In contrast to the ϕ6 P8, this protein does not have an essential role in penetration of the cytoplasmic membrane, as purified ϕ8 cores can infect sphaeroplasts (Sun et al., 2003). However, it could be involved in envelopment, as it anchors the membrane to the PC. The identity of this 11 kDa mass is not known.

Comparison of the ϕ6 virion and NC reconstructions revealed that the peripheral four-helix bundles of P8 that interact with P4 and form intertrimer interactions (Huiskonen et al., 2006a) are more disordered once the viral membrane has been removed (Figures 3A and 3B). A possible biological role for this domain is to facilitate NC disassembly during entry and membrane recognition during

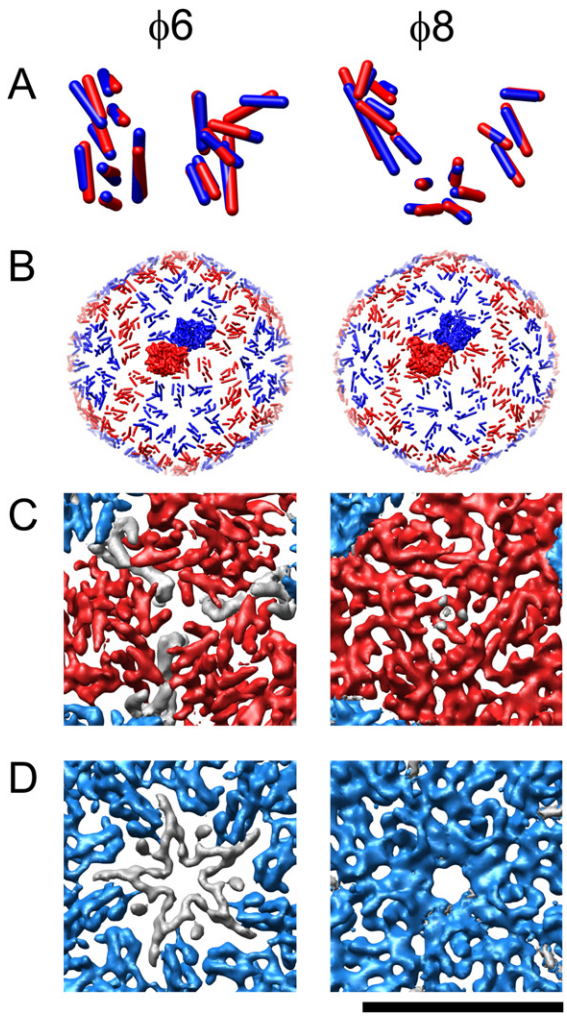

Figure 5. Comparison of P1 Tertiary and Quaternary Structure between ϕ6 and ϕ8

(A) An overlay of α helices between P1A (blue) and P1B (red) monomers is shown for both ϕ6 (left) and ϕ8 (right).

(B) The packing of α helices in the P1 shell is shown for ϕ6 (left) and ϕ8 (right).

(C) A close-up along the 3-fold axis of symmetry is shown for ϕ6 (left) and ϕ8 (right). The density assigned to P1 A and B monomers is in blue and red, respectively. The unassigned density is in gray.

(D) A close-up along the 5-fold axis of symmetry is shown for ϕ6 (left) and ϕ8 (right). The surfaces are colored as in (C). The isosurfaces were drawn at a high threshold ($\sim$3σ above the mean density) to reveal the structure in detail. The scale bar represents 10 nm in (C) and (D).

assembly. Temporal exposure of α helices has been observed for flock house virus and been suggested to play a role in disassembly (Bothner et al., 1998). A similar mechanism has been proposed for poliovirus interaction with cell membranes on entry, and is supported by recent structural data (Bubeck et al., 2005; Tosteson and Chow, 1997). In the case of ϕ6 entry, fusion of the viral membrane with the host's outer membrane could destabilize the P8 lattice, allowing insertion of the P8 α helices into the cytoplasmic membrane for the formation of a fusion pore, ultimately leading to the observed NC disassembly and the release of the polymerase complex (Romantschuk et al., 1988).

Organization of Packaged RNA

The spacing of the concentric RNA layers was observed to be related to the average packaging density. ϕ8 has the longest genome of all the cystoviruses (14,984 bp) (Hoogstraten et al., 2000; Mindich et al., 1999). For comparison, the ϕ6 genome is 13,385 bp in length (Gottlieb et al., 1988; McGraw et al., 1986; Mindich et al., 1988). The longer genome of ϕ8 results in tighter packing (2.9 nm average separation between the layers, which gives a calculated interhelix spacing of 3.3 nm, assuming hexagonal packing) than in ϕ6 (3.1 nm separation, interhelix spacing of 3.6 nm). ϕ8 has a packaging density of 399 mg/ml, compared to 357 mg/ml in ϕ6 (Huiskonen et al., 2006a) and 410 mg/ml in bluetongue virus (Gouet et al., 1999). The clarity of the RNA density, especially in the outermost layer, indicates that the inner surface of P1 imposes considerable order on the genome. The RNA becomes more disordered as it gets further away from the protein shell. Such ordering has also been observed in both electron cryomicroscopy and X-ray studies of rotavirus (Prasad et al., 1996), aquareovirus (Shaw et al., 1996), and bluetongue virus (Gouet et al., 1999).

Evolution of dsRNA Virus Capsids

We show here that the P1 α-helical tertiary structures are markedly different. At this resolution, we cannot rule out the possibility that the P1 topology is still conserved. However, genetic and biochemical studies support the hypothesis of significant structural divergence. Is the divergence also reflected in viral function and assembly? P1 can be considered to have three major roles: first as a scaffold onto which both the PC enzymes and the nucleocapsid protein attach, second as the site of RNA recognition and organization, and third as a metastable shell that through conformational changes is involved in the regulation of virus maturation. The scaffolding function of P1 in ϕ6 and ϕ8 has diverged so much that the whole nucleocapsid structure and envelope interactions are affected. Furthermore, there is some evidence that the P1 recognition site for the RNA pac site has diverged. For instance, the ϕ6 M segment cannot be acquired by ϕ8 (Mindich et al., 1999). Crosslinking studies have previously shown that the S segment binding site on the ϕ6 PC occurs between residues 98 and 155 (Qiao et al., 2003), where there is a 21 residue insertion in ϕ8 (Figure S2, ϕ8 residues 115–135). However, the PC's quaternary arrangement is still conserved: 60 copies of P1 form a dodecahedral cage with P1 pentamers filling the facets. The only other viruses to have 120 subunits in the innermost protein layer are also other dsRNA viruses (members of the *Totiviridae* and *Reoviridae* families). The arrangement of the mainly α-helical subunits, however, is different, with five monomers around the icosahedral 5-fold axis of symmetry and another five interdigitating between them (Grimes et al., 1998; Naitow et al., 2002; Nakagawa et al., 2003; Reinisch et al., 2000). Based

on the observation that the dsRNA virus inner capsid shell always seems to consist of 60 asymmetric dimers with a mainly α-helical fold, it has been speculated that they have in fact evolved from the same ancestor (Bamford et al., 2005; Naitow et al., 2002). If this is indeed the case, then the α-helical fold is much more flexible in evolutionary terms than the β-sheet jelly rolls that are strictly conserved in many different virus capsids. The metastable dodecahedral structure seen in the *Cystoviridae* PC may be related to its role in RNA packaging (Huiskonen et al., 2006a), a role which in the *Reoviridae* is accomplished with the help of nonstructural proteins (Taraporewala and Patton, 2004).

EXPERIMENTAL PROCEDURES

Specimen Preparation

Wild-type ϕ6 was propagated in *Pseudomonas syringae* HB10Y (Vidaver et al., 1973) and purified by rate-zonal centrifugation as described previously (Olkkonen et al., 1991). The virus was concentrated by pelleting in a Beckman airfuge (A100 rotor, 7 min, 29 psi, 18°C) and resuspended in 10 mM potassium phosphate (pH 7.5), 1 mM $MgCl_2$. Wild-type ϕ8 was propagated in *P. syringae* pv. *phaesolicola* LM2509 (Hoogstraten et al., 2000; Mindich et al., 1999). Exponential cultures were inoculated at a multiplicity of infection of 50–80 using a freshly prepared viral stock and incubated overnight at 15°C until the culture had lysed. This low temperature maximized the amount of the spike proteins in the viral preparation, as has been shown previously for ϕ6 (Mindich et al., 1979). The cell debris was removed by low-speed centrifugation, and the virus was concentrated by polyethylene glycol precipitation (0.5 M NaCl, 9% PEG 6000) and low-speed centrifugation. The PEG pellet was gently resuspended in 10 mM potassium phosphate (pH 7.5), 1 mM $MgCl_2$, 200 mM NaCl. As the pellets were extremely viscous, 0.05 mg/ml DNase I was also added during the resuspension step. The virus was purified by rate-zonal centrifugation (5%–20% sucrose in 10 mM potassium phosphate [pH 7.5], 1 mM $MgCl_2$, 200 mM NaCl, Sorvall AH629 rotor, 45 min, 24,000 rpm, 15°C), and the resulting light-scattering band was immediately concentrated in a Beckman airfuge (A100 rotor, 7 min, 29 psi, 18°C) and resuspended in 10 mM potassium phosphate (pH 7.5), 1 mM $MgCl_2$, 20 mM NaCl. The specific infectivity was 2×10^{11} pfu/mg. For core purification, the light-scattering band was concentrated (Sorvall T647.5 rotor, 43,000 rpm, 1 hr 5 min, 4°C) and resuspended in 10 mM potassium phosphate (pH 7.5), 1 mM $MgCl_2$, 20 mM NaCl. The viral envelope was then solubilized using a single Triton X-114 treatment, releasing cores that were purified by rate-zonal centrifugation (Bamford et al., 1995) (5%–20% sucrose in 20 mM Tris [pH 8], 7.5 mM $MgCl_2$, 50 mM NaCl, Sorvall TH660 rotor, 50 min, 29,000 rpm, 15°C) and the resulting light-scattering band was immediately concentrated in a Beckman airfuge (A100 rotor, 8 min, 29 psi, 18°C) and resuspended in 10 mM potassium phosphate (pH 7.5), 1 mM $MgCl_2$, 50 mM NaCl.

Electron Microscopy

Vitrified specimens from 3 μl droplets of the virus samples were prepared on holey carbon film (Quantifoil) as described previously (Adrian et al., 1984; Butcher et al., 1997). The specimens were imaged at −180°C under an FEI Tecnai F20 field emission gun transmission electron microscope using an Oxford CT3500 cryoholder. Micrographs were recorded on Kodak SO163 film under low dose conditions, at a nominal magnification of 50,000, and at several different defocus settings, in order to fill the nodes of the contrast transfer function later during the reconstruction (Table 1). The micrographs were developed in full-strength Kodak D19 film developer for 12 min.

Image Processing

Micrographs were scanned on a Zeiss Photoscan TD scanner at 7 μm intervals resulting in a nominal sampling of 1.4 Å pixel^{-1}. The data were binned to 2.8 Å pixel^{-1} sampling to facilitate processing. CTFFIND3 (Mindell and Grigorieff, 2003) was used to estimate the contrast transfer function parameters of the micrographs. Images with drift or astigmatism were discarded. ETHAN (Kivioja et al., 2000) was used to locate virus particles in the micrographs, and particle extraction was performed in EMAN (Ludtke et al., 1999). These images were contrast reversed and normalized for icosahedral reconstruction (Baker and Cheng, 1996; Crowther, 1971; Fuller et al., 1996). Bsoft (Heymann, 2001) was used in further image-processing steps.

Three-Dimensional Reconstruction

The 3D reconstruction of the ϕ6 nucleocapsid (Electron Microscopy Database [EMD], European Bioinformatics Institute [EBI] accession number EMD-1206; Huiskonen et al., 2006a) was used as a starting model to determine the orientations and origins of the ϕ6 virion and the ϕ8 core images in a model-based approach (Baker et al., 1999). PFT2 and EM3DR2 (Baker and Cheng, 1996) were used in the initial rounds of the refinement, and POR and P3DR (Ji et al., 2003; Marinescu et al., 2001) for subsequent rounds. Full contrast transfer function correction was applied when calculating the reconstructions in P3DR. The ϕ8 core reconstruction was used as the initial model for processing the ϕ8 virion images in a similar manner. The effective resolution of the models was estimated by splitting the particle images into two independent sets, calculating a reconstruction for both sets, and then calculating Fourier shell correlation (Harauz and van Heel, 1986) between the two reconstructions. The spatial frequency at which the correlation coefficient dropped below 0.5 was taken to represent the maximum resolution reached in the complete reconstruction. The resolution as a function of radius was estimated using the Fourier shell correlation of consecutive 2.8 nm thick shells as described previously (Huiskonen et al., 2004). Reconstruction statistics are listed in Table 1.

Visualization was carried out in UCSF Chimera, EMAN, and Bsoft (Heymann, 2001; Huang et al., 1996; Ludtke et al., 1999). The spacing of the ϕ8 RNA was calculated from a spherically averaged radial profile of the core reconstruction using Bsoft (Heymann, 2001). The ϕ8 P1 monomers were segmented manually in EMAN using the program qsegment (Ludtke et al., 1999). Masses were estimated in EMAN using a volume threshold of 1.5 standard deviations above the mean and a protein density of 1.35 g/ml (Ludtke et al., 1999).

Secondary-Structure Prediction

The P1 sequences from ϕ8, ϕ6, and ϕ13 (European Molecular Biology Laboratory accession numbers AAF63302.1, AAA32357.1, and AAG00446.1, respectively) were aligned using T-Coffee multiple sequence alignment (Notredame et al., 2000). The secondary structure for P1 was predicted by submitting this alignment to the Jpred server (Cuff and Barton, 2000). Putative α helices in the density map were identified using the program helixhunter (Jiang et al., 2001). The helices were aligned using LSQMAN (Kleywegt and Jones, 1995) to study the similarity of the P1 subunits.

Supplemental Data

Supplemental Data include two figures and can be found with this article online at http://www.structure.org/cgi/content/full/15/2/157/DC1/.

ACKNOWLEDGMENTS

The authors gratefully acknowledge the contributions of B. Koli for technical support, V. Kumar for his contribution to early work on the ϕ8 core, and R. Tuma for constructive comments. We thank the Electron Microscopy Unit of the Institute of Biotechnology, University of Helsinki, for providing microscopy facilities. The work was supported by the National Graduate School in Informational and Structural Biology (H.T.J. and J.T.H.), the Academy of Finland Centre of Excellence

Programme (2006–2011) (1213467 and 1112244, S.J.B.), and an Academy of Finland Research Fellowship (1208661, S.J.B.). As part of the European Science Foundation EUROCORES Programme EuroSCOPE, the work is also supported by funds from the European Commission's Sixth Framework Programme under contract ERAS-CT-2003-980409.

Received: September 27, 2006
Revised: December 21, 2006
Accepted: December 22, 2006
Published: February 13, 2007

REFERENCES

Abrescia, N.G., Cockburn, J.J., Grimes, J.M., Sutton, G.C., Diprose, J.M., Butcher, S.J., Fuller, S.D., San Martin, C., Burnett, R.M., Stuart, D.I., et al. (2004). Insights into assembly from structural analysis of bacteriophage PRD1. Nature *432*, 68–74.

Adrian, M., Dubochet, J., Lepault, J., and McDowall, A.W. (1984). Cryo-electron microscopy of viruses. Nature *308*, 32–36.

Baker, T.S., and Cheng, R.H. (1996). A model-based approach for determining orientations of biological macromolecules imaged by cryo-electron microscopy. J. Struct. Biol. *116*, 120–130.

Baker, T.S., Olson, N.H., and Fuller, S.D. (1999). Adding the third dimension to virus life cycles: three-dimensional reconstruction of icosahedral viruses from cryo-electron micrographs. Microbiol. Mol. Biol. Rev. *63*, 862–922.

Bamford, D.H., and Mindich, L. (1980). Electron microscopy of cells infected with nonsense mutants of bacteriophage ϕ6. Virology *107*, 222–228.

Bamford, D.H., Palva, E.T., and Lounatmaa, K. (1976). Ultrastructure and life cycle of the lipid-containing bacteriophage ϕ6. J. Gen. Virol. *32*, 249–259.

Bamford, D.H., Romantschuk, M., and Somerharju, P.J. (1987). Membrane fusion in prokaryotes: bacteriophage ϕ6 membrane fuses with the *Pseudomonas syringae* outer membrane. EMBO J. *6*, 1467–1473.

Bamford, D.H., Ojala, P.M., Frilander, M., Walin, L., and Bamford, J.K.H. (1995). Isolation, purification and function of assembly intermediates and subviral particles of bacteriophages PRD1 and ϕ6. In Microbial Gene Techniques, K.W. Adolph, ed. (San Diego: Academic Press), pp. 455–474.

Bamford, D.H., Grimes, J.M., and Stuart, D.I. (2005). What does structure tell us about virus evolution? Curr. Opin. Struct. Biol. *15*, 655–663.

Bothner, B., Dong, X.F., Bibbs, L., Johnson, J.E., and Siuzdak, G. (1998). Evidence of viral capsid dynamics using limited proteolysis and mass spectrometry. J. Biol. Chem. *273*, 673–676.

Bottcher, B., Wynne, S.A., and Crowther, R.A. (1997). Determination of the fold of the core protein of hepatitis B virus by electron cryomicroscopy. Nature *386*, 88–91.

Bubeck, D., Filman, D.J., Cheng, N., Steven, A.C., Hogle, J.M., and Belnap, D.M. (2005). The structure of the poliovirus 135S cell entry intermediate at 10-angstrom resolution reveals the location of an externalized polypeptide that binds to membranes. J. Virol. *79*, 7745–7755.

Butcher, S.J., Bamford, D.H., and Fuller, S.D. (1995). DNA packaging orders the membrane of bacteriophage PRD1. EMBO J. *14*, 6078–6086.

Butcher, S.J., Dokland, T., Ojala, P.M., Bamford, D.H., and Fuller, S.D. (1997). Intermediates in the assembly pathway of the double-stranded RNA virus ϕ6. EMBO J. *16*, 4477–4487.

Butcher, S.J., Grimes, J.M., Makeyev, E.V., Bamford, D.H., and Stuart, D.I. (2001). A mechanism for initiating RNA-dependent RNA polymerization. Nature *410*, 235–240.

Caldentey, J., and Bamford, D.H. (1992). The lytic enzyme of the *Pseudomonas* phage ϕ6. Purification and biochemical characterization. Biochim. Biophys. Acta *1159*, 44–50.

Conway, J.F., Cheng, N., Zlotnick, A., Wingfield, P.T., Stahl, S.J., and Steven, A.C. (1997). Visualization of a 4-helix bundle in the hepatitis B virus capsid by cryo-electron microscopy. Nature *386*, 91–94.

Crowther, R.A. (1971). Procedures for three-dimensional reconstruction of spherical viruses by Fourier synthesis from electron micrographs. Philos. Trans. R. Soc. Lond. B Biol. Sci. *261*, 221–230.

Cuff, J.A., and Barton, G.J. (2000). Application of multiple sequence alignment profiles to improve protein secondary structure prediction. Proteins *40*, 502–511.

Daugelavicius, R., Cvirkaite, V., Gaidelyte, A., Bakiene, E., Gabrenaite-Verkhovskaya, R., and Bamford, D.H. (2005). Penetration of enveloped double-stranded RNA bacteriophages ϕ13 and ϕ6 into *Pseudomonas syringae* cells. J. Virol. *79*, 5017–5026.

de Haas, F., Paatero, A.O., Mindich, L., Bamford, D.H., and Fuller, S.D. (1999). A symmetry mismatch at the site of RNA packaging in the polymerase complex of dsRNA bacteriophage ϕ6. J. Mol. Biol. *294*, 357–372.

Dryden, K.A., Wieland, S.F., Whitten-Bauer, C., Gerin, J.L., Chisari, F.V., and Yeager, M. (2006). Native hepatitis B virions and capsids visualized by electron cryomicroscopy. Mol. Cell *22*, 843–850.

Fuller, S.D., Butcher, S.J., Cheng, R.H., and Baker, T.S. (1996). Three-dimensional reconstruction of icosahedral particles—the uncommon line. J. Struct. Biol. *116*, 48–55.

Gottlieb, P., Metzger, S., Romantschuk, M., Carton, J., Strassman, J., Bamford, D.H., Kalkkinen, N., and Mindich, L. (1988). Nucleotide sequence of the middle dsRNA segment of bacteriophage ϕ6: placement of the genes of membrane-associated proteins. Virology *163*, 183–190.

Gottlieb, P., Strassman, J., Qiao, X.Y., Frucht, A., and Mindich, L. (1990). In vitro replication, packaging, and transcription of the segmented double-stranded RNA genome of bacteriophage ϕ6: studies with procapsids assembled from plasmid-encoded proteins. J. Bacteriol. *172*, 5774–5782.

Gottlieb, P., Potgieter, C., Wei, H., and Toporovsky, I. (2002a). Characterization of ϕ12, a bacteriophage related to ϕ6: nucleotide sequence of the large double-stranded RNA. Virology *295*, 266–271.

Gottlieb, P., Wei, H., Potgieter, C., and Toporovsky, I. (2002b). Characterization of ϕ12, a bacteriophage related to ϕ6: nucleotide sequence of the small and middle double-stranded RNA. Virology *293*, 118–124.

Gouet, P., Diprose, J.M., Grimes, J.M., Malby, R., Burroughs, J.N., Zientara, S., Stuart, D.I., and Mertens, P.P. (1999). The highly ordered double-stranded RNA genome of bluetongue virus revealed by crystallography. Cell *97*, 481–490.

Grahn, A.M., Butcher, S., Bamford, J.K.H., and Bamford, D.H. (2006). PRD1—dissecting the genome, structure and entry. In The Bacteriophages, R. Calendar, ed. (New York: Oxford University Press), pp. 161–170.

Grimes, J.M., Burroughs, J.N., Gouet, P., Diprose, J.M., Malby, R., Zientara, S., Mertens, P.P., and Stuart, D.I. (1998). The atomic structure of the bluetongue virus core. Nature *395*, 470–478.

Grünewald, K., Desai, P., Winkler, D.C., Heymann, J.B., Belnap, D.M., Baumeister, W., and Steven, A.C. (2003). Three-dimensional structure of herpes simplex virus from cryo-electron tomography. Science *302*, 1396–1398.

Hantula, J., and Bamford, D.H. (1988). Chemical crosslinking of bacteriophage ϕ6 nucleocapsid proteins. Virology *165*, 482–488.

Harauz, G., and van Heel, M. (1986). Similarity measures between images. Exact filters for general geometry of 3D reconstructions. Optik *73*, 146–156.

Heymann, J.B. (2001). Bsoft: image and molecular processing in electron microscopy. J. Struct. Biol. *133*, 156–169.

Hoogstraten, D., Qiao, X., Sun, Y., Hu, A., Onodera, S., and Mindich, L. (2000). Characterization of ϕ8, a bacteriophage containing three

double-stranded RNA genomic segments and distantly related to ϕ6. Virology *272*, 218–224.

Huang, C.C., Couch, G.S., Pettersen, E.F., and Ferrin, T.E. (1996). Chimera: an extensible molecular modeling application constructed using standard components. Pacific Symposium on Biocomputing *1*, 724.

Huiskonen, J.T., Kivelä, H.M., Bamford, D.H., and Butcher, S.J. (2004). The PM2 virion has a novel organization with an internal membrane and pentameric receptor binding spikes. Nat. Struct. Mol. Biol. *11*, 850–856.

Huiskonen, J.T., de Haas, F., Bubeck, D., Bamford, D.H., Fuller, S.D., and Butcher, S.J. (2006a). Structure of the bacteriophage ϕ6 nucleocapsid suggests a mechanism for sequential RNA packaging. Structure *14*, 1039–1048.

Huiskonen, J.T., Jäälinoja, H.T., Briggs, J.A.G., Fuller, S.D., and Butcher, S.J. (2006b). Structure of a hexameric RNA packaging motor in a viral polymerase complex. J. Struct. Biol., in press. Published online October 7, 2006. 10.1016/j.jsb.2006.08.021.

Ji, Y., Marinescu, D.C., Zhang, W., and Baker, T.S. (2003). Orientation refinement of virus structures with unknown symmetry. In Proceedings of the 17th International Symposium on Parallel and Distributed Processing (Nice, France: IEEE Press), http://ieeexplore.ieee.org/xpls/abs_all.jsp?arnumber=1213138.

Jiang, W., Baker, M.L., Ludtke, S.J., and Chiu, W. (2001). Bridging the information gap: computational tools for intermediate resolution structure interpretation. J. Mol. Biol. *308*, 1033–1044.

Johnson, M.D., III, and Mindich, L. (1994). Isolation and characterization of nonsense mutations in gene 10 of bacteriophage ϕ6. J. Virol. *68*, 2331–2338.

Kainov, D.E., Butcher, S.J., Bamford, D.H., and Tuma, R. (2003a). Conserved intermediates on the assembly pathway of double-stranded RNA bacteriophages. J. Mol. Biol. *328*, 791–804.

Kainov, D.E., Pirttimaa, M., Tuma, R., Butcher, S.J., Thomas, G.J., Jr., Bamford, D.H., and Makeyev, E.V. (2003b). RNA packaging device of double-stranded RNA bacteriophages, possibly as simple as hexamer of P4 protein. J. Biol. Chem. *278*, 48084–48091.

Kakitani, H., Iba, H., and Okada, Y. (1980). Penetration and partial uncoating of bacteriophage ϕ6 particle. Virology *101*, 475–483.

Kenney, J.M., Hantula, J., Fuller, S.D., Mindich, L., Ojala, P.M., and Bamford, D.H. (1992). Bacteriophage ϕ6 envelope elucidated by chemical cross-linking, immunodetection, and cryoelectron microscopy. Virology *190*, 635–644.

Kivioja, T., Ravantti, J., Verkhovsky, A., Ukkonen, E., and Bamford, D. (2000). Local average intensity-based method for identifying spherical particles in electron micrographs. J. Struct. Biol. *131*, 126–134.

Kleywegt, G.J., and Jones, T.A. (1995). Where freedom is given, liberties are taken. Structure *3*, 535–540.

Laurinavicius, S., Kakela, R., Bamford, D.H., and Somerharju, P. (2004). The origin of phospholipids of the enveloped bacteriophage ϕ6. Virology *326*, 182–190.

Laurinmäki, P.A., Huiskonen, J.T., Bamford, D.H., and Butcher, S.J. (2005). Membrane proteins modulate the bilayer curvature in the bacterial virus Bam35. Structure *13*, 1819–1828.

Lisal, J., and Tuma, R. (2005). Cooperative mechanism of RNA packaging motor. J. Biol. Chem. *280*, 23157–23164.

Lisal, J., Kainov, D.E., Bamford, D.H., Thomas, G.J., Jr., and Tuma, R. (2004). Enzymatic mechanism of RNA translocation in double-stranded RNA bacteriophages. J. Biol. Chem. *279*, 1343–1350.

Ludtke, S.J., Baldwin, P.R., and Chiu, W. (1999). EMAN: semiautomated software for high-resolution single-particle reconstructions. J. Struct. Biol. *128*, 82–97.

Makeyev, E.V., and Bamford, D.H. (2000a). The polymerase subunit of a dsRNA virus plays a central role in the regulation of viral RNA metabolism. EMBO J. *19*, 6275–6284.

Makeyev, E.V., and Bamford, D.H. (2000b). Replicase activity of purified recombinant protein P2 of double-stranded RNA bacteriophage ϕ6. EMBO J. *19*, 124–133.

Mancini, E.J., Kainov, D.E., Grimes, J.M., Tuma, R., Bamford, D.H., and Stuart, D.I. (2004). Atomic snapshots of an RNA packaging motor reveal conformational changes linking ATP hydrolysis to RNA translocation. Cell *118*, 743–755.

Marinescu, D.C., Ji, Y., and Lynch, R.E. (2001). Space-time tradeoffs for parallel 3D reconstruction algorithms for atomic virus structure determination. Concurrency Computat. Pract. Exper. *13*, 1083–1106.

McGraw, T., Mindich, L., and Frangione, B. (1986). Nucleotide sequence of the small double-stranded RNA segment of bacteriophage ϕ6: novel mechanism of natural translational control. J. Virol. *58*, 142–151.

Mettenleiter, T.C., Klupp, B.G., and Granzow, H. (2006). Herpesvirus assembly: a tale of two membranes. Curr. Opin. Microbiol. *9*, 423–429.

Mindell, J.A., and Grigorieff, N. (2003). Accurate determination of local defocus and specimen tilt in electron microscopy. J. Struct. Biol. *142*, 334–347.

Mindich, L. (2004). Packaging, replication and recombination of the segmented genome of bacteriophage ϕ6 and its relatives. Virus Res. *101*, 83–92.

Mindich, L., Sinclair, J.F., and Cohen, J. (1976). The morphogenesis of bacteriophage ϕ6: particles formed by nonsense mutants. Virology *75*, 224–231.

Mindich, L., Lehman, J., and Huang, R. (1979). Temperature-dependent compositional changes in the envelope of ϕ6. Virology *97*, 171–176.

Mindich, L., Nemhauser, I., Gottlieb, P., Romantschuk, M., Carton, J., Frucht, S., Strassman, J., Bamford, D.H., and Kalkkinen, N. (1988). Nucleotide sequence of the large double-stranded RNA segment of bacteriophage ϕ6: genes specifying the viral replicase and transcriptase. J. Virol. *62*, 1180–1185.

Mindich, L., Qiao, X., Qiao, J., Onodera, S., Romantschuk, M., and Hoogstraten, D. (1999). Isolation of additional bacteriophages with genomes of segmented double-stranded RNA. J. Bacteriol. *181*, 4505–4508.

Naitow, H., Tang, J., Canady, M., Wickner, R.B., and Johnson, J.E. (2002). L-A virus at 3.4 Å resolution reveals particle architecture and mRNA decapping mechanism. Nat. Struct. Biol. *9*, 725–728.

Nakagawa, A., Miyazaki, N., Taka, J., Naitow, H., Ogawa, A., Fujimoto, Z., Mizuno, H., Higashi, T., Watanabe, Y., Omura, T., et al. (2003). The atomic structure of rice dwarf virus reveals the self-assembly mechanism of component proteins. Structure *11*, 1227–1238.

Notredame, C., Higgins, D.G., and Heringa, J. (2000). T-Coffee: a novel method for fast and accurate multiple sequence alignment. J. Mol. Biol. *302*, 205–217.

Olkkonen, V.M., Gottlieb, P., Strassman, J., Qiao, X.Y., Bamford, D.H., and Mindich, L. (1990). In vitro assembly of infectious nucleocapsids of bacteriophage ϕ6: formation of a recombinant double-stranded RNA virus. Proc. Natl. Acad. Sci. USA *87*, 9173–9177.

Olkkonen, V.M., Ojala, P.M., and Bamford, D.H. (1991). Generation of infectious nucleocapsids by in vitro assembly of the shell protein on to the polymerase complex of the dsRNA bacteriophage ϕ6. J. Mol. Biol. *218*, 569–581.

Poranen, M.M., and Tuma, R. (2004). Self-assembly of double-stranded RNA bacteriophages. Virus Res. *101*, 93–100.

Poranen, M.M., Paatero, A.O., Tuma, R., and Bamford, D.H. (2001). Self assembly of a viral molecular machine from purified protein and RNA constituents. Mol. Cell *7*, 845–854.

Poranen, M.M., Tuma, R., and Bamford, D.H. (2005). Assembly of double-stranded RNA bacteriophages. Adv. Virus Res. *64*, 15–43.

Prasad, B.V., Rothnagel, R., Zeng, C.Q., Jakana, J., Lawton, J.A., Chiu, W., and Estes, M.K. (1996). Visualization of ordered genomic

RNA and localization of transcriptional complexes in rotavirus. Nature *382*, 471–473.

Qiao, X., Qiao, J., Onodera, S., and Mindich, L. (2000). Characterization of ϕ13, a bacteriophage related to ϕ6 and containing three dsRNA genomic segments. Virology *275*, 218–224.

Qiao, X., Qiao, J., and Mindich, L. (2003). Analysis of specific binding involved in genomic packaging of the double-stranded-RNA bacteriophage ϕ6. J. Bacteriol. *185*, 6409–6414.

Reinisch, K.M., Nibert, M.L., and Harrison, S.C. (2000). Structure of the reovirus core at 3.6 Å resolution. Nature *404*, 960–967.

Romantschuk, M., and Bamford, D.H. (1985). Function of pili in bacteriophage ϕ6 penetration. J. Gen. Virol. *66*, 2461–2469.

Romantschuk, M., Olkkonen, V.M., and Bamford, D.H. (1988). The nucleocapsid of bacteriophage ϕ6 penetrates the host cytoplasmic membrane. EMBO J. *7*, 1821–1829.

Shaw, A.L., Samal, S.K., Subramanian, K., and Prasad, B.V. (1996). The structure of aquareovirus shows how the different geometries of the two layers of the capsid are reconciled to provide symmetrical interactions and stabilization. Structure *4*, 957–967.

Spear, P.G., and Longnecker, R. (2003). Herpesvirus entry: an update. J. Virol. *77*, 10179–10185.

Stitt, B.L., and Mindich, L. (1983). The structure of bacteriophage ϕ6: protease digestion of ϕ6 virions. Virology *127*, 459–462.

Sun, Y., Qiao, X., Qiao, J., Onodera, S., and Mindich, L. (2003). Unique properties of the inner core of bacteriophage ϕ8, a virus with a segmented dsRNA genome. Virology *308*, 354–361.

Taraporewala, Z.F., and Patton, J.T. (2004). Nonstructural proteins involved in genome packaging and replication of rotaviruses and other members of the *Reoviridae*. Virus Res. *101*, 57–66.

Tosteson, M.T., and Chow, M. (1997). Characterization of the ion channels formed by poliovirus in planar lipid membranes. J. Virol. *71*, 507–511.

Trus, B.L., Gibson, W., Cheng, N., and Steven, A.C. (1999). Capsid structure of simian cytomegalovirus from cryoelectron microscopy: evidence for tegument attachment sites. J. Virol. *73*, 2181–2192.

van Etten, J., Lane, L., Gonzalez, C., Partridge, J., and Vidaver, A. (1976). Comparative properties of bacteriophage ϕ6 and ϕ6 nucleocapsid. J. Virol. *18*, 652–658.

Vidaver, A.K., Koski, R.K., and Van Etten, J.L. (1973). Bacteriophage ϕ6: a lipid-containing virus of *Pseudomonas phaseolicola*. J. Virol. *11*, 799–805.

Whittaker, G.R., Kann, M., and Helenius, A. (2000). Viral entry into the nucleus. Annu. Rev. Cell Dev. Biol. *16*, 627–651.

Yang, H., Makeyev, E.V., and Bamford, D.H. (2001). Comparison of polymerase subunits from double-stranded RNA bacteriophages. J. Virol. *75*, 11088–11095.

Yang, H., Makeyev, E.V., Butcher, S.J., Gaidelyte, A., and Bamford, D.H. (2003). Two distinct mechanisms ensure transcriptional polarity in double-stranded RNA bacteriophages. J. Virol. *77*, 1195–1203.

Zhou, Z.H., He, J., Jakana, J., Tatman, J.D., Rixon, F.J., and Chiu, W. (1995). Assembly of VP26 in herpes simplex virus-1 inferred from structures of wild-type and recombinant capsids. Nat. Struct. Biol. *2*, 1026–1030.

Zhou, Z.H., Chen, D.H., Jakana, J., Rixon, F.J., and Chiu, W. (1999). Visualization of tegument-capsid interactions and DNA in intact herpes simplex virus type 1 virions. J. Virol. *73*, 3210–3218.

Accession Numbers

The reconstructions have been deposited in the Electron Microscopy Database at the European Bioinformatics Institute with the accession numbers EMD-1301 (ϕ6 virion), EMD-1299 (ϕ8 virion), and EMD-1300 (ϕ8 core).